Check for
updates

Unparalleled coupled ocean-atmosphere summer heatwaves in the New Zealand region: drivers, mechanisms and impacts

M. James Salinger, et al. *[full author details at the end of the article]*

Abstract

During austral summers (DJF) 1934/35, 2017/18 and 2018/19, the New Zealand (NZ) region (approximately 4 million km^2) experienced the most intense coupled ocean-atmosphere heatwaves on record. Average air temperature anomalies over land were + 1.7 to 2.1 °C while sea surface temperatures (SST) were 1.2 to 1.9 °C above average. All three heatwaves exhibited maximum SST anomalies west of the South Island of NZ. Atmospheric circulation anomalies showed a pattern of blocking centred over the Tasman Sea extending south-east of NZ, accompanied by strongly positive Southern Annular Mode conditions, and reduced trough activity over NZ. Rapid melt of seasonal snow occurred in all three cases. For the two most recent events, combined ice loss in the Southern Alps was estimated at 8.9 km^3 (22% of the 2017 volume). Sauvignon blanc and Pinot noir wine grapes had above average berry number and bunch mass in 2018 but were below average in 2019. Summerfruit harvest (cherries and apricots) was 14 and 2 days ahead of normal in 2017/18 and 2018/19 respectively. Spring wheat simulations suggested earlier flowering and lower grain yields compared to average, and below-average yield and tuber quality in potatoes crops occurred. Major species disruption occurred in marine ecosystems. Hindcasts indicate that the heatwaves were either atmospherically driven or arose from combinations of atmospheric surface warming and oceanic heat advection.

1 Introduction

Kidson ([1935](#)) described the first documented austral summer (DJF) heatwave covering the New Zealand (NZ) area in 1934/35, with regional temperature anomalies over land averaging + 1.7 °C compared to the 1981–2010 normal. At the time, this event was so unusual, almost 3 °C warmer than other 1930s summers; it was described as 'remarkably warm'. Salinger et al. ([2019a](#)) documented the unprecedented austral summer (DJF) 2017/18 heatwave covering the NZ region.

Regional average air (over land) and sea surface temperature anomalies were + 2.2 °C and + 1.9 °C, respectively. Numerous terrestrial and marine impacts persisted for the entire austral summer resulting in the (1) largest loss of glacier ice in the Southern Alps since 1962; (2) early Sauvignon blanc wine-grape maturation; and (3) major species disruption in marine ecosystems. Various atmospheric drivers were identified, and the event was associated with very low wind speeds, reduced upper ocean mixing and heat fluxes from the atmosphere to the ocean causing substantial warming of the stratified surface layers of the Tasman Sea. In 2018/19, New Zealand again experienced a very warm summer, although not as intense as the 1934/35 or 2017/18 events.

Using the Hobday et al. (2016) definition of marine heat waves (MHW), Oliver et al. (2018) found a 54% increase in the number of MHW days globally since the early twentieth century with an increase of 3–9 days per decade in the NZ region. From two general circulation model (GCM) ensembles, Perkins-Kirkpatrick et al. (2018) concluded that a Tasman Sea MHW with the intensity of the 2017/18 event would have been virtually impossible without anthropogenic warming. The atmospheric blocking that was responsible for the prolonged period of high mean sea level pressure (MSLP) also displayed some anthropogenic influence, although Perkins-Kirkpatrick et al. (2018) note that this detected influence was less than that on the sea surface temperature.

MHWs are caused by a range of processes at different spatial and temporal scales, from localized air–sea heat flux to large-scale climate drivers such as the El Niño Southern Oscillation (ENSO; Benthuysen et al. 2014; Heidemann and Ribbe 2019) and Southern Annular Mode (SAM; Thompson et al. 2011). Behrens et al. (2019) investigated mechanisms of MHWs in the Tasman Sea using a forced global ocean sea-ice model and Argo observations, concluding that they are largely controlled by meridional heat transport from the subtropics through the interchange between the East Australian Current and the Tasman Front. One contributor to the increased frequency of MHWs (Oliver et al. 2018) has been regional warming trends. Sutton and Bowen (2019) documented a 0.1 to 0.3 °C per decade increase in ocean temperatures since 1981 with warming penetrating from the surface to 200 m depth around coastal NZ and to at least 850 m in the eastern Tasman Sea.

This study examines the three most intense atmospheric heatwaves (AHW) and associated MHW for the NZ region covering the austral summers of 1934/35, 2017/18 and 2018/19. It diagnoses the atmospheric and oceanic drivers, impacts on marine and terrestrial ecosystems, including viticulture and arable cropping. Monthly to decadal atmospheric and oceanic mechanisms were investigated, along with an assessment of future likelihood of similar events.

2 Methods

Many of the methods used here were described in Salinger et al. (2019a). They are outlined briefly here, with new approaches described in more detail.

2.1 Observations of atmosphere and ocean temperature

The 22-station NZ air temperature (NZ22T) series (Salinger et al. 1992) was used to calculate monthly mean air temperature anomalies for 1934–2019, relative to the 1981–2010 normal. From daily time series, extreme statistics TX90p (percentage of days when the daily maximum temperature is above the 90th percentile), TN90p (percentage of days when the daily minimum temperature is above the 90th percentile) and number of summer days ≥ 25 °C averaged over New

Zealand during 1940–2019 were calculated as in Salinger et al. (2019a). Eight stations were analysed for the 1934/35 event. Monthly sea surface temperature (SST) observations were obtained from Extended Reconstructed Sea Surface Temperature version 5 (ERSST; Huang et al. 2017).

For the NZ exclusive economic zone (NZEEZ), an area-weighted temperature anomaly was calculated from SST and land surface temperatures. The $2° \times 2°$ ERSST product from 34° to 48°S, and 165° to 179°E (Fig. 2g) was combined with NZ22T to produce a new temperature series: the NZEEZT series for 1930–2019.

Daily SST estimates came from the NOAA ¼° daily Optimum Interpolation SST analysis (daily OISST) on a 0.25° latitude/longitude grid spanning September 1981–July 2019 as in Salinger et al. (2019a). These were averaged over 160–172° E and 35–45° S (Fig. 2g). Daily 9 am measurements of SST were obtained since 1953 at the Portobello Marine Laboratory (PML) in Otago Harbour, South Island, NZ. The Hobday et al. (2016, 2018) MHW definitions were applied to identify and characterise MHWs based on daily SST measurements from the daily OISST and PML datasets as in Salinger et al. (2019a). Ocean sub-surface temperature from GODAS (Saha et al. 2006) were averaged between 40° S and 45° S, 140° E and 150° W, over depths 25 to 600 m, and Argo profiles (Jayne et al. 2017) were extracted for the eastern Tasman Sea (160–172° E, 35–45° S).

2.2 Atmospheric circulation

For atmospheric circulation, monthly mean sea level pressures (MSLP) and 500-hPa geopotential heights were obtained from the NCEP/NCAR Reanalysis (Kistler et al. 2001) and the ERA-Interim reanalysis (Dee et al. 2011). Several indices were used to characterize the circulation: Trenberth (1976) Z1 and M1 indices and weather regimes over NZ (Kidson 2000) for the 2017/18 and 2018/19 heatwaves. Z1 measures west-east (zonal) flow and M1 south-north (meridional) flow in the NZ region: negative Z1 is typical in blocking situations when the prevailing westerly to south-westerly flow is absent in the region, especially with negative M1 (northerly flow anomaly). For large-scale circulation and monthly to decadal modes of variability, the following were used: the Fogt et al. (2009) Southern Annular Mode (SAM) reconstructed index, combined with the Marshall (2003) SAM index, the Southern Oscillation Index (SOI) of Troup (1965) and for the Interdecadal Pacific Oscillation (IPO) the tripole index (Henley et al. 2015).

A subset of past analogue (similar) three-month periods was chosen from both the ERA-Interim and twentieth century reanalysis (20CR, Compo et al. 2011). Analogues were selected for each of the three summers based on anomaly correlation and root mean-squared difference (RMSD) using 500 hPa anomaly fields over the NZ/Tasman Sea region. Analogues that exhibited anomaly correlations of at least 0.65 and RMSD of 19 geopotential metres (gpm) or less were selected. For 1934/35, the RMSD threshold was reduced to 16 gpm to reduce the number of analogue cases to a comparable level to the later summers. A total of eight 20CR analogues were chosen for 1934/35, while 11 and 10 ERA-Interim analogues were chosen for 2017/18 and 2018/19 respectively. A t test was used to estimate the significance of average SAM and SOI indices in the analogue samples chosen.

2.3 Ocean hindcasts

The global ocean model hindcast for this study was as described in Salinger et al. (2019a). The climatology for 2000–2018 was used to remove the seasonal signal. Heat content anomalies

were computed over the mixed layer depth, defined by a density difference of 0.01 kg/m^3 from the surface.

2.4 Glaciers and seasonal snow

The end of summer snowline (EOSS) time series (Chinn et al. 2012) was used to estimate Southern Alps mountain glacier mass balance from 1977 to 2018 for EOSS$_{Alps}$ (Salinger et al. 2019a). Regression relationships were employed to calculate EOSS$_{Alps}$ for 1935 and 2019, using Hermitage Mt Cook glacier season annual mean temperature, the SAM index and Kidson (2000) Trough and Block regimes frequencies (Salinger et al. (2019b). EOSS$_{Brewster}$ was estimated from satellite imagery and regression relations between EOSS$_{Alps}$ and EOSS$_{Brewster}$ to derive a value for 2019. The methods of Chinn et al. (2012) were used to estimate downwasting and proglacial lake growth.

Estimates of water stored as seasonal snow in the South Island for 2017–2018 and 2018–2019 were provided by the model 'SnowSim', available through Meridian Energy Ltd. (*https://www.meridianenergy.co.nz/who-we-are/our-power-stations/snow-storage/*; Garr and Fitzharris 1996). SnowSim calculates water stored as seasonal snow for key hydro-generating river catchments and is tuned to their long-term water balance. Past estimates are in general agreement with historical observations of snow back to 1930. Estimates for seasonal snow for 1934–1935 are given in Fitzharris and Garr (1995) and de Lautour (1999).

2.5 Agriculture

2.5.1 Horticulture

Grapes The impact of grapevine phenology was predicted using the Grapevine Flowering Véraison (GFV) model (Parker et al. 2013) and harvest is defined when sugar reaches a concentration of 200 g/L (Parker 2012). Meteorological data (March 1947 to April 2019) were sourced from the Marlborough Regional Station (41.48° S; 173.95° E). Observations of yield component data over ten seasons (2010 to 2019) were obtained from Marlborough commercial vineyards (Pinot noir $n = 13$; Sauvignon blanc $n = 34$). Inflorescence numbers per metre of row were collected shortly after budburst in November and bunch and berry mass shortly before harvest. Berry number per bunch was calculated from bunch and berry mass data.

Summer fruit Harvest dates were gathered for one variety of cherry ('Lapins') and two varieties of apricots ('Nzsummer 2' and 'Nzsummer3') at the Plant and Food Research orchard in Clyde, Central Otago (45.20° S 169.32° E) for 2016–2019, where meteorological data were also obtained.

2.5.2 Arable

Wheat The Agricultural Production Systems sIMulator (APSIM; Holzworth et al. 2014) was used to assess the performance of spring wheat during the three summers 1934/35, 2017/18 and 2018/19, against climate in the current normal period (1981–2010). Simulations were set for a key wheat-producing area (Lincoln, Canterbury; 43.62° S 172.47° E) by assuming that crops were fully irrigated and fertilized, to minimize the effects of additional yield-limiting

factors in the assessment. The production metrics considered were flowering time, cycle length, grain yield and frequency of heat stress events during the reproductive period, when wheat crops are sensitive to yield-damage by short periods above threshold temperatures (Supplementary Material). No observed crop data were available.

Potatoes A preliminary study sought early evidence of how the 2017/18 heatwave affected potato production in NZ (Siano et al. 2018) at three sites: Ohakune in the central North Island (39.50° S, 175.45° E; 563 m above sea level (masl)) which was irrigated, Opiki, south west North Island (40.46° S, 175.48° E; 4 masl) which was rain-fed, and Hastings, eastern North Island (39.62° S, 176.73° E; 8 masl) which was irrigated. For the 2018/19 season, two locally bred (Ilam Hardy and Rua), and five offshore bred (Agria, Hermes, Taurus, Snowden and Fianna) processing cultivars were trialled at the three sites. Physiological data (net photosynthesis, transpiration rate and stomatal conductance) were measured at specific growth stages of the crop, while yield and tuber quality data were determined at final harvest.

2.6 Marine ecosystems

Impacts on marine ecosystems were evaluated from published data describing immediate losses of bull kelp (*Durvillaea* spp.) and associated community changes, and new data describing bull kelp community recovery 1.5 years after the 2017/18 MHW. Impacts on bull kelp and its community were estimated by comparing drone images and abundance surveys of benthic species, respectively, before and after the 2017/18 MHW from Oaro (− 42.52° S, 173.51° E), Pile Bay (43.62° S, 172.76° E), and Moeraki (45.36° S, 170.86° E). A disturbance simulation experiment initiated in a bull kelp forest at Oaro in June 2017 was re-sampled in August 2019 to provide new data on bull kelp recovery and community change. Finally, at Pile Bay, we collected new before/after MHW data (where bull kelp canopy had been lost) to quantify changes in abundances of other canopy-forming seaweeds (see S1 and Thomsen et al. 2019 and Thomsen and South 2019).

3 Results

3.1 Observations of atmosphere and oceans

3.1.1 Surface temperatures

The coupled ocean-atmosphere heatwaves in the NZ region during the three summer seasons studied here were the most intense recorded in the NZ and Tasman Sea regions in 150 years of land-surface air temperature records, and ~ 40 years of satellite-derived SST records (Sutton and Bowen 2019), as shown in Fig. 1a–f.

For all three heatwaves, both land air and sea surface temperatures were 1.2° to 1.6 °C above the DJF 1981–2010 averages over the entire region (Salinger and Diamond 2020), from 32° to 52°S, 150° E to 180° (Table 1 and Figs. 1and 2g). NZ22T anomalies (Table 1) were 1.7 °C, 2.1 °C and 1.2 °C (Fig. 1a and Table 1), by far the three warmest on record (Salinger 1979; Mullan et al. 2010). Indices of temperature extremes for NZ (Table 1 and Fig. 1b) show that the percentages of summer warm days above the 90th percentile were 26%, 33% and 22%,
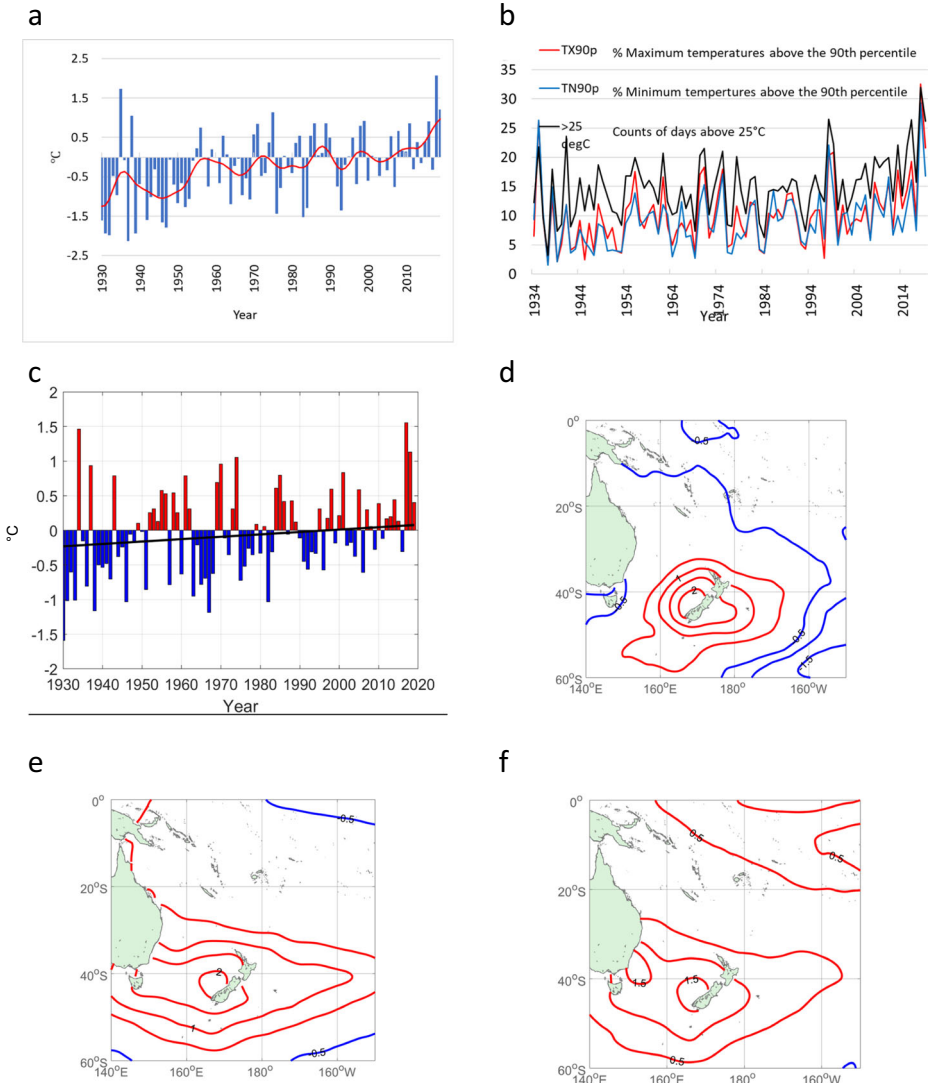
Fig. 1 **a** New Zealand 22 station air temperatures (NZ22T) series (red smoothed) 1930–2019. **b** Extremes—TX90p, TN90p and days > 25 °C averaged over New Zealand 1940–2019. **c** New Zealand region SST (34° S–48° S, 166° E–180° E) from ERSSTv5. **d**–**f** SST DJF from ERSSTv5. **d**. 1934/35. **e** 2017/18. **f** 2018/19. **All anomalies are from the 1981–2010 climatology period**

and percentages of warm nights above the 90th percentile were 26%, 29% and 17%. Counts of summer days ≥ 25 °C averaged 22, 32 and 26 days nationwide for the three seasons.

For the Tasman Sea and east of NZ (32°–52° S, 150°–180° E), the MHWs were characterised by SSTs 1.5 °C, 1.9 °C and 1.2 above average (Fig. 1d–f), the largest anomalies on record. All three showed a similar spatial pattern with highest anomalies to the west of the South Island of NZ. The largest departures from average occurred in DJF for 1934/35 and 2017/18 but in JFM for 2018/19.

Table 1 Indices for the three heatwaves. NZ22T is the 22 station NZT series for surface temperature over the land area of New Zealand, ERSST is the ERSST version 5 for the New Zealand (NZ) Exclusive Economic Zone, 34 to 48° S, and 165° to 179° E, and NZEEZT are NZ22Tand ERSST combined and weighted for the entire NZ region with anomalies in °C

Metric	1934/35	2017/18	2018/19
NZ22T	*1.73*	*2.07*	*1.21*
ERSSTv5	*1.46*	*1.92*	*1.15*
NZEEZ	*1.48*	*1.92*	*1.15*
SAM	*1.45*	*2.20*	1.08
SOI	− 0.1	0.7	*2.9*
IPO	− 0.16	*− 0.92*	0.09
Z1	*− 16*	− 15	− 7
M1	*− 40*	8	− 5
Trough		2	3
Kidson Zonal		−9	4
Block		8	− 7
Warm days TX90p	*26*	*33*	*22*
Warm nights TN90p	*26*	*29*	*17*
Days ≥ 25 °C	*22*	*32*	*26*

All temperature departures are anomalies from the 1981–2010 climatology period. NZ22T mean − 0.18 °C, standard deviation (s.d) of ± 0.70 °C, ERSST mean − 0.03, s.d ± 0.36 °C and NZEEZT mean − 0.04 s.d ± 0.37 °C. SAM the Southern Annular Mode (Fogt et al. (2009) mean 0.04, s.d 1.63, SOI the Troup (1965) Southern Oscillation Index mean 0.0, s.d 1.3 and the Interdecadal Pacific Oscillation (IPO) the tripolar index (Henley et al. 2015) mean − 0.9, s.d. 0.83, Z1 (mean − 0.4 s.d. 16) and M1 (mean − 1.7, s,d, 25) are Trenberth (1976) zonal and meridional indices. Kidson regimes are Trough, Zonal and Block anomalies (Kidson 2000). TX90p and TN90p are the percentages of days above the maximum (TX) and minimum (TN) daily 90 percentiles (mean is 10% 1981–2010 climatology period, with days ≥ 25 °C counts ≥ 25 °C, all averaged for 26 NZ climate stations. Mean counts days ≥ 25 °C 15.0, s.d ± 5.2 days. Italic values are significant at $p < 0.05$

Applying a MHW definition (Hobday et al. 2016) to daily OISST for the eastern Tasman Sea (Fig. 2a, g) showed that the 2018/19 event had a similar duration but reduced intensity compared to the 2017/18 event. During summer 2017/18, the eastern Tasman Sea experienced MHW conditions for 138 days (consisting of two distinct periods of 99 days and 39 days), peaking as a category IV (extreme) MHW (Hobday et al. 2018) with a maximum intensity of 4.1 °C. In comparison, the 2018/19 event lasted for 137 days, peaking as a category II (strong) MHW, with a maximum intensity of 2.8 °C. Nearshore surface waters at the PML followed a similar pattern (Fig. 2b), experiencing MHW conditions for several short (7–28 days) periods interspersed with cooler breaks. However, maximum anomalies during summer 2018/19 (2.6 °C) were approximately half those observed during summer 2017/18 (5.7 °C) (Salinger et al. 2019a).

3.1.2 Atmospheric circulation

The three DJF seasons (Fig. 3a–c) show a pattern of blocking (higher than normal pressures): in 1934/35 and 2017/18, to the east and southeast of NZ, with negative pressure anomalies northwest of NZ, while 2018/19 had the strongest positive pressure anomalies over the central Tasman Sea. The M1 and Z1 circulation indices showed northerly airflow for 1934/35, and easterly airflow for 1934/35 and 2017/18. Airflow was northeasterly for 2018/19. Kidson weather regimes showed a lack of trough types in late spring (NDJ) together with lack of zonal regimes and more blocking throughout the season for 2017/18. In contrast, 2018/19 had fewer blocking regimes, but more of the zonal regime.
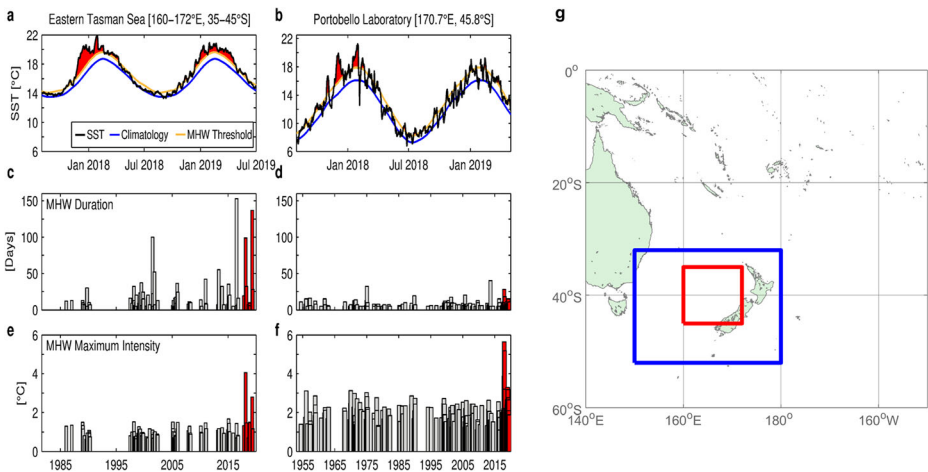
Fig. 2 (First row) Time series of sea surface temperature (SST) climatology (1981–2011; blue), 90th percentile MHW threshold (orange) and summer 2017/18 to 2018/19 SSTs (black) from the **a** eastern Tasman Sea (160–172° E, 35–45° S) and **b** the Portobello Marine Laboratory (45.88° S, 170.5° E). The red shaded regions identify periods associated with MHWs from each location using the Hobday et al. (2016) definition. The red shaded regions identify periods associated with MHWs detected in the SST time series from each location using the Hobday et al. [2018] definition. (Second row) The duration of each MHW detected in the SST time series for the **c** eastern Tasman Sea and **d** Portobello Marine Laboratory. The red shaded region highlights MHWs detected between October 2017 and July 2019. (Third row) As above but showing the maximum intensity of each MHW detected in the SST time series for **e** the eastern Tasman Sea and **f** Portobello Marine Laboratory. (Right). **g** Areas used for SST anomalies for the New Zealand region (blue) and eastern Tamsan Sea (red)

The 500-hPa geopotential height anomalies were consistent (Fig. 3d–f) with very strong blocking in the Tasman Sea extending southeast of NZ. The 1934/35 had an average positive height anomaly of 30 gpm west of the North Island over the north Tasman Sea. The 2017/18 anomaly was the most intense, 60 gpm to the south east of the South Island, whereas the 2018/19 anomaly was 40 gpm over the western Tasman Sea. The 1934/35 and 2018/19 events all exhibited ridges east and south east of the South Island.

Over austral spring and summer 1934/35, the SAM was positive (Table 1). The SAM was also positive during 2017/18 and 2018/19. ENSO activity was weak in 1934/35 (SOI −0.1) and in 2017/18 (SOI +0.7). The 2018/19 event was in the La Niña phase (SOI +2.9). The last would on average be associated with northerly quarter airflow anomalies in spring, and north easterly airflow anomalies over NZ in summer (Gordon 1986). Only in summer 2017/18 was the IPO index negative, and the extremely positive SAM (+2.2) for the season may have influenced the SSTs in the NZ region used to calculate the Tripole index.

3.1.3 Analogue seasons

The DJF 1934/35 anticyclone had a maximum anomaly of 30 gpm northwest of NZ (Fig. 3d). The positive anomalies covered a wide area across most of NZ and, from the east coast of NZ to 155° W at an average of about 10 gpm. The position (northwest of NZ as opposed to southeast), extent and intensity of this anticyclone was less than that for DJF 2017/18 season (Fig. 3e, Salinger et al. 2019a). Compared
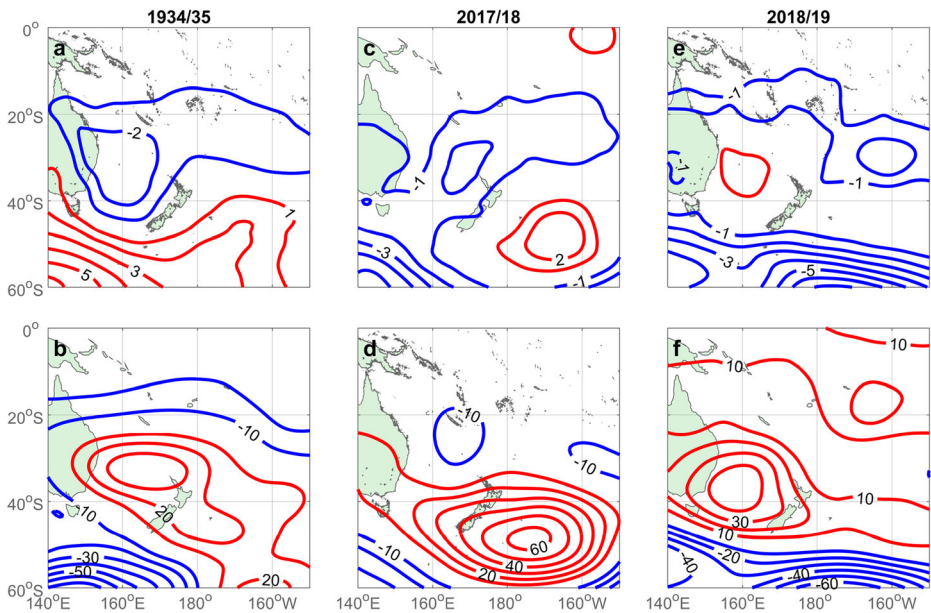
Fig. 3 Atmospheric circulation patterns. DJF mean sea level pressure anomaly: **a** 1934/35, **c** 2017/18 and **e** 2018/19. DJF 500-hPa Geopotential Height anomaly: **b** 1934/35, **d** 2017/18 and **f** 2018/19

with the analogue cases exhibiting similar spatial patterns of circulation anomalies (Table 2(a)), the DJF 1934/35 SAM value (1.45) was higher than all but two of the analogue cases (Table 2(a)). The DJF 2017/18 season exhibited a strong SAM value of + 2.20 (Salinger et al. 2019a) which falls in the middle of distribution of analogue seasons.

The DJF 2018/19 (Fig. 3f) anticyclone anomaly reached a maximum of + 40 gpm centred northwest of NZ. The position and extent of the positive height anomaly differed from 2017/18 and its intensity was considerably less. The SAM value for DJF 2018/19 (+ 1.08), while positive, was not statistically significant and was third lowest compared to the selection of analogue seasons. Therefore, the SAM likely did not play such a strong role in DJF 2018/19 and this may have contributed to the reduced warmth of the 2018/19 summer. In contrast, La Niña conditions in the equatorial Pacific (SOI of + 7.4) would on average have been associated with warm SST anomalies in the Tasman Sea. For 2017/18, blocking weather types (Kidson 2000) were most prevalent with a lack of the zonal regime and the analogue seasons displayed a dominance of the blocking regime. In comparison, 2018/19 zonal types were prevalent. In both cases, analogues exhibited a lack of the troughing regime.

3.1.4 Ocean sub-surface temperature

GODAS sub-surface ocean temperature patterns for DJF 2017/18 and 2018/19 for 40–45° S (Fig. 4) indicate very shallow positive anomalies west of the South Island, with a narrow band down to about 50 m east of the South Island. Positive SST anomalies also existed in the western Tasman Sea and into the south Pacific east of NZ. These were also shallow but far more intense in 2018/19 to the south east of Australia, but

Table 2 Detailed 500-hPa analogue results by season. These are the results of an analysis of the atmospheric circulation patterns were compared using anomaly correlation and root mean-square difference over the region 135° E–140° W, 65° S–25° S (see text) compared to (a) 1934/35, (b) 2017/18 and (c) 2018/19 season. Italicized are significant values ($p < 0.05$) for SAM and SOI(/10), and 10 or 90 percentiles for Z1, M1 and Kidson regimes

Season	SAM value	SOI value	Z1 value	M1 value	Trough	Kidson Zonal	Block
OND 1915	−0.95	*−0.2*	12	*−28*			
JFM 1935	*1.00*	0.4	−10	−35			
FMA 1935	*−0.50*	*0.3*	*−23*	−35			
SON 1965	*1.35*	−1.6	−15	−9	1	13	−14
JFM 1966	−1.25	−1.2	−5	−23	−3	−7	10
AMJ 1978	*0.30*	0.4	*−40*	−10	*11*	−7	*−4*
JJA 1979	2.61	*−0.3*	−14	−34	−16	6	11
NDJ 1981	*−0.50*	0.5	13	−20	*1*	*−8*	**7**
AMJ 2003	2.10	−0.9	3	−12	−7	3	5
Mean Value	0.46	−0.29	−9	−23	−2	0	3
DJF 1935	*1.45*	*−0.3*	*−16*	−40			
JJA 1979	2.61	*−0.3*	−14	−34	−10	3	7
OND 1981	−0.52	−0.1	11	−35	−13	2	11
JJA 1985	*1.06*	−0.2	−3	−33	−5	−3	8
DJF 1994	2.39	−0.1	1	−37	−4	−2	
FMA 1999	2.70	*1.2*	8	−35	*−13*	−9	*22*
MAM 1999	2.74	*1.0*	−3	−41	*−18*	7	*11*
JAS 2005	0.02	*−0.2*	8	−10	−10	9	1
DJF 2008	2.70	*1.7*	*−19*	−22	−10	*−11*	*21*
DJF 2013	*1.20*	−0.8	1	0	−6	5	1
JFM 2018	*1.70*	4.5	−10	0	1	*−11*	10
Mean Value	1.66	0.67	−4	−20	−11	−1	10
DJF 2018	*2.20*	*0.7*	−15	8	2	−9	8
JFM 1982	−1.72	*0.3*	12	−15	1	−3	6
JJA 1993	*2.15*	−1.6	18	*−33*	*−13*	21	*−8*
DJF 1995	*0.77*	−0.8	−14	9	*−15*	11	4
AMJ 1999	*2.32*	0.7	−6	1	*−11*	7	4
MJJ 1999	*1.60*	*0.2*	0	45	*−13*	16	−3
DJF 2013	*1.20*	−0.8	1	−22	−6	5	1
NDJ 2015	2.52	−2.2	−7	3	−10	3	7
DJF 2016	*2.21*	−3.3	−5	1	−10	5	5
FMA 2016	*1.85*	−3.2	1	−38	*−15*	−17	−2
NDJ 2018	*2.01*	2.9	*−17*	−24	0	6	−6
Mean Value	1.49	−0.78	−2	−7	−9	9	1
DJF 2019	1.08	2.9	−7	−5	3	4	−7

not around NZ, than in 2017/18. The Argo measurements (Fig. 4c) averaged over the eastern Tasman Sea confirmed surface warming from December to February, peaking at 3 °C mean anomaly in 2017/18 and 1.5 °C in 2018/19. The anomaly was shallow, mainly confined to the upper 20 m when it formed, and both deepened slightly as they were eroded from the surface.

3.1.5 Ocean hindcasts

The MHW in 2015/16 which affected the region east of Tasmania (Fig. 5a) was documented by Oliver et al. (2017) and attributed to enhanced heat transport in the East Australian Current Extension (EAC-Ext). Modelled SST anomalies were intensified south of 35° S along the east coast of Australia and Tasmania and exceeded 1 °C. Positive SST anomalies were also present in the Tasman Front region, while the remaining Tasman Sea was characterised by negative SST anomalies. Mixed layer heat content anomalies show a pattern consistent with the SST anomalies, along the flow path of the EAC-Ext. where summer mixed layers are around 20 m
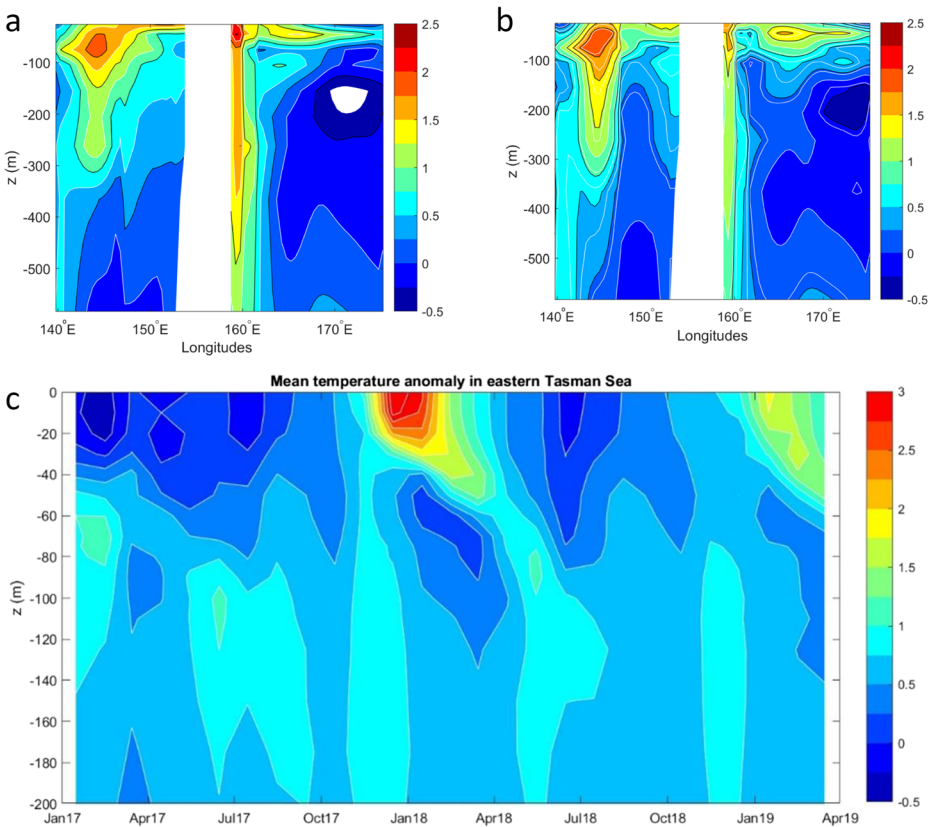
Fig. 4 Subsurface sea temperature anomalies. **a**, **b** GODAS subsurface Tasman Sea. **a** DJF 2017/18 and **b** DJF 2018/19. **c** Subsurface temperature anomalies in the eastern Tasman Sea from Argo floats January 2017–April 2019

deep. In comparison to the 2015/16 event, the 2017/18 heat wave was more intense, with SST anomalies above 2 °C over large parts of the Tasman Sea. The mixed layer heat content anomaly was positive over the entire Tasman Sea but showed a different spatial pattern compared to the SST anomalies, which implies differences in the driving mechanism compared to the 2015/16 MHW. The 2017/18 event was predominantly atmospherically driven, with low wind speeds reducing the vertical mixing of heat into the water column and causing a shallow but intense surface warming. As the surface layer warmed, the mixed layers became shallower, and mixed layer heat content anomalies were reduced. This differs from cases where oceanic heat advection is dominant and mixed layer remain shallow, as in the case of the 2015/16 and 2018/19 MHW where SST and mixed layer heat content anomalies show similar patterns. The warming in 2018/19 extended from the EAC-Ext. region over the Southern Tasman Sea to the coastal waters of eastern NZ, and along the Chatham Rise. Each MHW event is affected by a different combination of both surface warming and oceanic heat advection drivers (Behrens et al. 2019).

Interannual variability in Tasman Sea SST, mixed layer heat content and winds speed anomalies are illustrated in Fig. 5g. While the period from 2003 to 2012 was predominantly characterised by negative mixed layer heat content anomalies and negative SST anomalies,
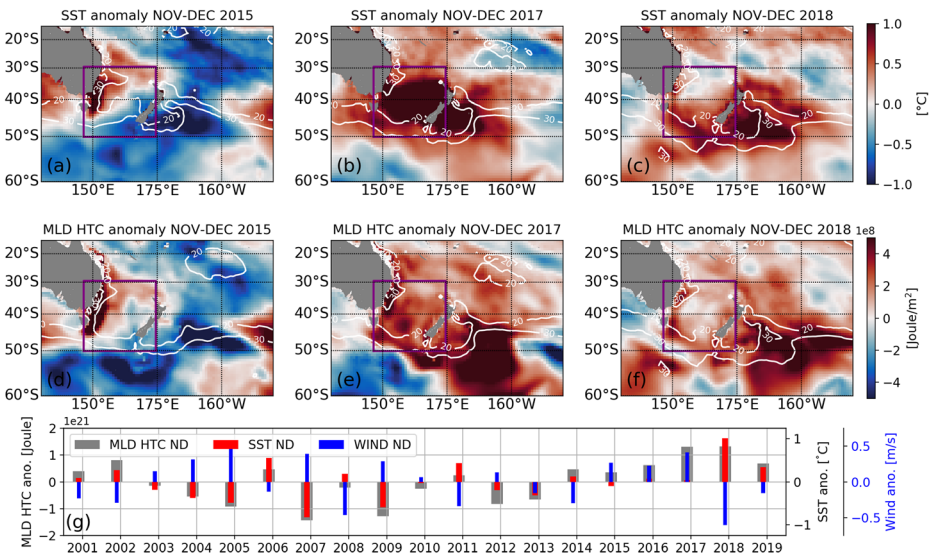
Fig. 5 Modelled SST anomalies (**a**–**c**) for November–December 2015, 2017 and 2018 in °C. The white contour lines show the mixed layer depths with 10 m intervals. Mixed layer heat content anomaly (**d**–**f**) for the same period in Joule/m². **g** Timeseries of integrated or averaged anomalies over the Tasman Sea between 145° E, 175° E, 50° S, 30° S for November–December. Grey, red and blue bars show integrated mixed layer heat content anomalies in Joule, average SST anomalies in °C, and average wind speed anomalies m/s, respectively

generally positive anomalies have been evident since then. The positive wind anomalies in 2015, 2016 and 2017 with increased vertical mixing prevented the development of significant SST anomalies during spring.

3.2 Glaciers and seasonal snow

3.2.1 Glaciers

Ice volume loss in the Southern Alps for the small and medium glaciers was estimated to be 3.2 km³ water equivalent (w.e.) in 1934/35, 3.6 km³ in 2017/18 and 3.2 km³ in 2018/19. This totals 10 km³ w.e. for the three heatwave summers, 19% of the total ice volume of the Southern Alps in the 1977 inventory (Chinn 2001). For the two consecutive heatwave summers, losses amounted to 6.8 km³. Total ice loss (small and medium plus 12 large glaciers) came to 8.9 km³. or an accumulated 22% of the 2017 volume, the largest for the entire period back to 1962 (Fig. 6a).

3.2.2 Seasonal snow

The 1934–1935 snow year was remarkable. Water stored as seasonal snow reached a maximum that was just below average at 402 mm w.e. in mid-October, based on SnowSim model estimates. Rapid snowmelt began in mid-November and all snow had disappeared by 11 January, the third earliest date for the period 1930 to 2019 (de Lautour 1999). Melt rate over this period was 6.5 mm/d w.e., the highest of the three summers. The earliest date for disappearance of all seasonal snow is 28
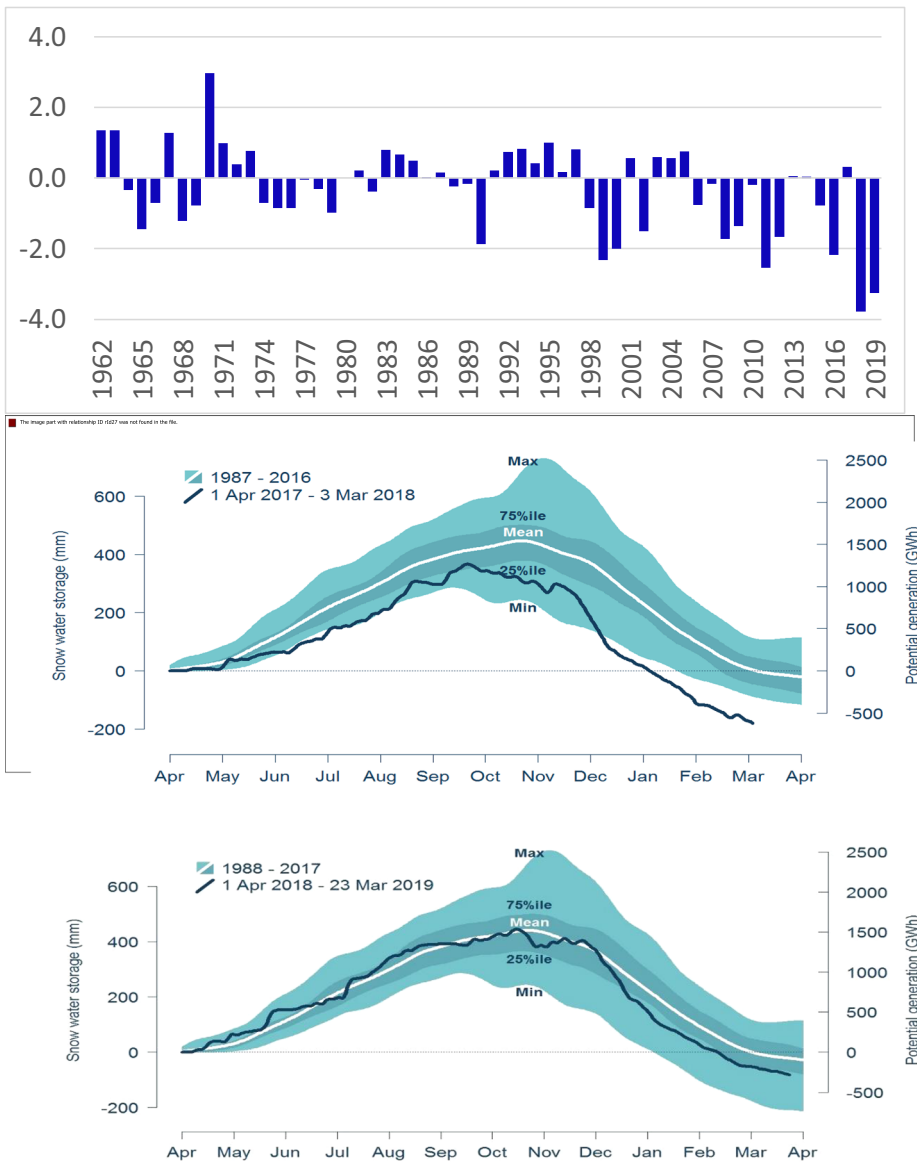
Fig. 6 Southern Alps ice volume and seasonal snow. **a** Southern Alps ice volume change (km³), between years, for all glaciers of the Southern Alps from 1962 to 2019. **b, c** Estimated water stored as seasonal snow (mm) from SnowSim for the period 1987–2019

December for the 1974–75 snow year, but this was from a maximum of only 198 mm w.e., among the lowest since 1930.

During the 2017–2018 snow year, the estimated water stored as seasonal snow leading up to August (Fig. 6b) was very low. It reached a maximum of 30% of average at 350 mm w.e. in late September, much earlier than usual. Rapid melt began on 18 November and from mid-December 2018 the snowpack was the lowest on record. By 10 January, all the seasonal snow

had melted, the second earliest date since 1930, with extraordinary loss of permanent glacier snow and ice. Melt rate over this period was 5.7 mm/d w.e.

SnowSim estimated that maximum accumulation for the 2018–2019 snow year was close to average at 420 mm w.e. and occurred in late October (Fig. 6c), slightly later than normal. There was rapid melt from late November, but it took until 12 February for all the seasonal snow to disappear. Melt rate over this period was 5.0 mm/d w.e.

3.3 Agriculture

3.3.1 Horticulture

Grapes Temperatures in Marlborough were above the 1981–2010 climatology for the 2017–2018 and 2018–2019 seasons (Table 1: supplementary Fig. S1), particularly at the key phenological stages of inflorescence initiation (in the season before harvest), flowering and early fruit development (in the current season, Tables 3 and 4). Above-average temperatures at initiation and flowering were reflected in higher Pinot noir inflorescence number per metre of row and berry number per bunch (Pinot noir and Sauvignon blanc). Berry mass was reduced (Tables 3 and 4) supporting industry observations that the Marlborough 2019 harvest was in general less than anticipated (Gregan 2019). Probable environmental drivers were multiple daily maximum temperatures greater than 30 °C in the first 6 weeks of 2019. High temperature shock is reported to inhibit photosynthesis (Greer and Weston 2010) and water stress during the initial phase of berry development is reported to significantly reduce final berry mass (Ojeda et al. 2001). The GFV model simulations of flowering, véraison and harvest dates advanced since 1948 (Fig. 7) and the advances of last two seasons reflected the above average temperatures during spring (Tables 3 and 4). Despite the earlier véraison and harvest dates, mean temperatures during the ripening period did not increase (Fig. 1a), unlike increases observed elsewhere (Molitor and Junk 2019). This possibly reflects the temperate climate of Marlborough and the abrupt changes in temperature that may occur between concurrent phenophases of vine development during the season (Fig. S1).

Table 3 Key phenological stages for wine grapes, temperature and yield data. Timing of key phenological stages and temperatures at and between those stages

Harvest year	Date			Mean daily temperature at key phenology times (°C)		Mean daily temperature between key phenology times (°C)		
	Flowering	Véraison	20° Brix	Initiation[a]	Flowering[a]	1 Sept to flowering	Flowering to véraison	Véraison to 20° Brix
Long-term average (1987–2017)	5 Dec	15 Feb	21 Mar	17.6	17.3	12.9	17.7	16.9
2018	30 Nov	2 Feb	5 Mar	17.9	18.6	13.6	19.7	19.0
2019	2 Dec	6 Feb	12 Mar	18.7	18.5	13.3	19.1	17.6

[a] Initiation temperatures occur in the season before harvest, flowering temperatures are in the season of harvest. Dates used to estimate temperatures at this time are Dec 14 to Jan 17 and Dec 9 to Jan 9 for initiation and flowering respectively (Trought 2005)

Table 4 Sauvignon blanc and Pinot noir yield component data

	Average (2010–19)	Cv[a] 2010–2019	Vintage 2018	Vintage 2019
Pinot noir				
Average bunch mass (g)	113.8	25.0	131.9 (6.5)[b]	76.4 (4.2)
Average berry mass (g)	1.50	13.02	1.85 (0.04)	1.19 (0.02)
Average berry number per bunch	39.6	13.37	46.5 (3.5)	38.9 (3.1)
Inflorescence number per m row	24.4	19.7	25.9 (0.8)	28.1 (0.7)
Sauvignon blanc				
Average bunch mass (g)	144.4	16.3	183.4 (3.58)	131.3 (3.63)
Average berry mass (g)	2.05	8.15	2.37 (0.04)	1.78 (0.04)
Average berry number per bunch	70.9	12.7	78.2 (1.3)	74.9 (2.4)
Inflorescence number per m row	29.3	14.0	29.3 (0.6)	30.0 (0.8)

[a] *cv* coefficient of variation

[b] Numbers in brackets are the standard error of the mean

Summerfruit Of the four seasons' data available, September to January temperature departures from normal during 2016–2019 were 0.0, − 0.5, + 2.2 and + 0.6 °C. For the cherry variety, 2018 and 2019 harvest dates were 13 and 3 days respectively ahead of 2016 (a normal season). For apricots, the two heatwave summers were 14 and 2 days ahead of normal.

3.3.2 Arable

Wheat APSIM-wheat simulations showed a reduction in grain yields during heatwave years by up to 9% compared to an estimated median historical of ~ 9 t/ha (Fig. 8). During heatwave years, there was a more frequent occurrence of shorter cycles, earlier flowering and risk of heat stress events throughout the reproductive phase than the historical average for Lincoln.

Potatoes Heat and moisture stress were evident in Ohakune and Opiki (central and western North Island) and Hastings (eastern North Island) in 2017/18. In Opiki and Hastings, there were supra-optimal temperatures (> 25 °C) for 54 and 60 days, respectively. Potato tubers from each site revealed that yield was primarily affected by the increase in the volume of unmarketable or defective tubers that reached up to 85% of the total volume of tubers collected. This was due largely to the incidence of an array of tuber physiological defects such as enlarged lenticels, growth cracks, netting, malformations and second growths.

For the 2018/19 season in Opiki and Hastings, the number of days > 25 °C were 103 and 61 days respectively (Fig. S3), with sub-optimal rainfall in Opiki (423 mm) (Table S2, supplementary material). In Opiki and Hastings, site average harvest index, total and marketable yield were reduced by up to 11.7%, 43.3% and 45.2%, respectively, with reference to the cooler environment of Ohakune. The total number of tubers per plant and percentage of large- and medium-sized tubers (> 50 mm) declined. Dry matter content was also down by 15.7%. The elevated temperatures in Hastings resulted in increases in plant height and total plant leaf area, suggesting an enhanced dry matter partitioning to the haulm promoting vegetative growth (Levy and Veilleux 2007). It also increased the transpiration rate and stomatal conductance. Conversely, the water deficit in Opiki suppressed vegetative growth and stomatal conductance. These conditions led to a decrease in net photosynthesis by as much as 16.5%. The increase in the volume of unmarketable or defective tubers was

Fig. 7 Predicted Marlborough Sauvignon blanc **a** flowering, **b** véraison, **c** 20° Brix dates using GFV phenology model (Parker et al. 2013). **d** Mean daily temperature during ripening véraison to 20° Brix. The fitted lines are **a** $y = 228.4 - 0.065x$, R_2 0.124; **b** $y = 371 - 0.101x$, R_2 0.141; **c** $y = 418 - 0.107x$, R_2 0.096; **d** $y = 19.56 - 0.0013x$, R_2 0.0005. Note: the late phenology in 1993 coincided with the Mt Pinatubo volcanic eruption
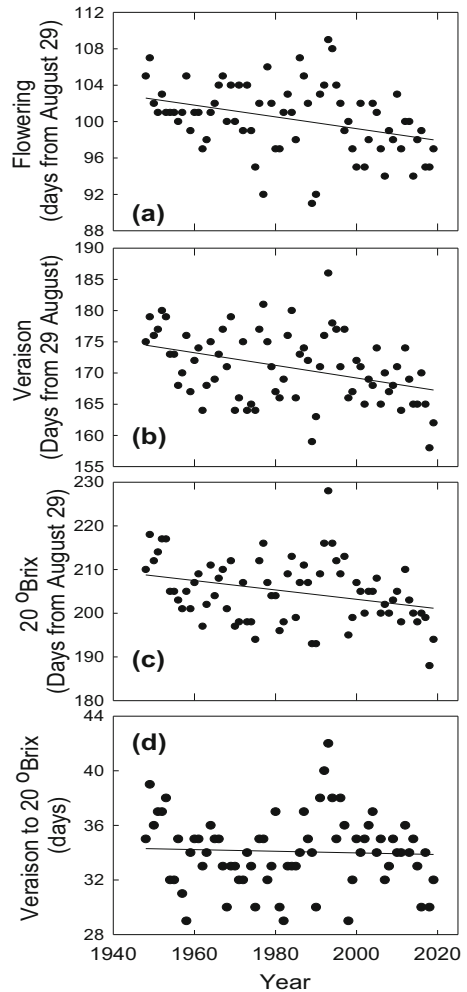
dramatic (up to 44%) which significantly reduced economic yield. The defective tubers exhibited physiological defects attributed to heat and moisture stress (Fig. S4). The most common defect was second growth in the form of heat sprouts (in-field sprouting), chained tubers and gemmation because of elevated soil temperatures and moisture stress (Hiller and Thornton 2008). Second growth was most common in Hastings (18.5%) and Opiki (16.8%) with extreme heat events, and lower in Ohakune (9.7%), which is cooler.

The result of the trial showed location-specific adaptations (agronomic zoning) among the tested commercial potato cultivars. Hermes performed well in the drought-prone conditions of Opiki but performance was reduced in the hotter condition of Hastings, while Snowden performed better in Hastings than in Opiki. Further analysis showed that 'Taurus', was the most stable and adaptable cultivar across test environments during the 2018/19 season (Fig. S5).
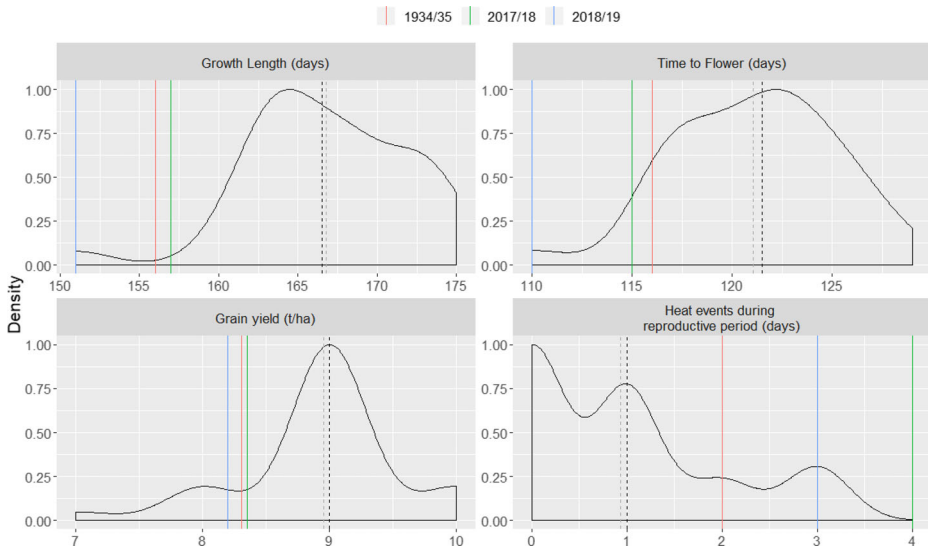
(1981-2010).

Fig. 8 Simulated physiological responses of irrigated spring wheat during three heatwave years (1934/35, 2017/18 and 2018/19) in Lincoln, Canterbury, New Zealand. Dashed lines are the median (black) and average (dark-grey) of 30 years (1981–2010)

3.4 Marine ecosystems

Dramatic losses of bull kelp were reported immediately after the 2017/18 MHW, with 100% loss of *Durvillaea poha* at Pile Bay where SST exceeded 23 °C (Thomsen et al. 2019; Thomsen and South 2019). Cascading effects included losses of mussels and colonization of ephemeral seaweeds (including the invasive kelp *Undaria pinnatifida*). Furthermore, *Undaria* and other ephemeral seaweeds colonized plots that had lost bull kelp in Moeraki and Oaro (Thomsen et al. 2019; Thomsen and South 2019). New data showed that bull kelp cover was reduced by 60% in the undisturbed control plots in the Oaro disturbance simulation experiment. Only 1.3% of the pre-MHW juvenile bull kelp survived and no new recruits were found in the disturbed plots, with bull kelps being replaced by red and green turf algae. Bull kelp remained absent from Pile Bay and nearby reefs in Lyttelton Harbour, 1.5 years after the 2017/18 MHW. After the 2017/18 MHW, plots previously inhabited by bull kelp were dominated by *Undaria* in the lower zone (43% cover) in winter months. Also, native perennial canopy-forming species (including *Hormosira banksii*, *Carpophyllum maschalocarpum* and *Cystophora scalaris* and *Cystopohora torulosa*) had recruited in 88% of the plots after the MHW and the loss of bull kelp (see S1 for more details).

4 Discussion and conclusions

Heatwaves are becoming a major impact of global warming with the Intergovernmental Panel on Climate Change 5th Assessment Report (Hartmann et al. 2013) indicating likely increases in unusually warm days and nights across most continents, and several occurrences of MHWs

in 2019 (Blunden and Arndt 2019). The unprecedented heatwave in the 2017/18 austral summer, coupled with a combined AHW/MHW event (Salinger et al. 2019a) was one example. Although Perkins-Kirkpatrick et al. (2018) suggests that the 2017/18 MHW would have been 'virtually impossible' without an anthropogenic influence, the 1934/35 event indicates a similar episode has occurred in the past which was only 0.3 °C cooler, without any allowance for anthropogenic global warming (AGW). Hence, it is important to examine similar AHW/MHWs in the NZ region in the climate record to document drivers and impacts.

Three such austral summer events occurred—in decreasing order of magnitude 2017/18, 1934/35 and 2018/19. The heatwaves had very similar atmospheric and oceanic footprints, covering all the land area, the entire central and south Tasman Sea and across to 180° E in the southwest Pacific. Mid-tropospheric (500-hPa) anomalies were extremely similar with strong blocking in the Tasman Sea extending south east of NZ. The 2017/18 event appeared predominantly atmospherically driven. Behrens et al. (2019) note each MHW is unique, either atmospherically driven, or a combination of atmospheric surface warming and oceanic heat advection. Trenberth et al. (2019) suggest that MHWs in the Tasman Sea region may be linked to heat transports from the South Pacific to the Indian Ocean north of Australia via the Indonesian Throughflow. Increased advection of warmer waters into the Tasman Sea is likely to be at the expense of a weak heat transport between the Pacific and Indian basins. As the inter-basin flow relaxes during El Niño years, the southward extension of the EAC is enhanced contributing to warming in the southern Tasman Sea.

Projected circulation changes for the late twenty-first century (Mullan et al. 2016) show MSLP increases during DJF, especially to the southeast of NZ. The airflow over the country becomes more northeasterly, and at the same time associated with more (possibly blocking) anticyclones and lacking in troughs. There is also a trend towards the positive SAM resulting in higher MSLPs in the NZ region, but this depends on interplay with stratospheric ozone recovery (Arblaster et al. 2011). These are all features displayed in the 2017/18 and 2018/19 heatwaves, with circulation regimes and their analogues exhibiting a lack of the troughing regime. Given that the Tasman Sea mixed layer heat content anomalies are in recent years have been above average, it appears likely that human-induced warming has played a significant role in the two recent coupled ocean-atmospheric heatwaves.

All three heatwaves produced significant impacts on glaciers and seasonal snow and ice, and on terrestrial and marine ecosystems. Ice loss in small and medium glaciers has been estimated to range from 3.2 to 3.6 km^3 in each event. Across all three heatwave summers, there was an accumulated ice volume loss of 22% of the 2017 volume. In all three cases, SnowSim showed swift snowmelt commencing in mid-November and completing very early. Melt rates ranged between 5.0 mm/d w.e. (2018/19) and 6.5 mm/d w.e. (1934/35) making 1934/35 the most remarkable.

For grapes in Marlborough, above average temperatures resulted in higher than average inflorescence numbers, and in 2018, berry number and bunch mass for Sauvignon blanc and Pinot noir wine grapes. However, 2019 berry and bunch mass were reduced, reflecting unusually high temperatures (over 30 °C) and vine water stress. The heat waves experienced in the past two growing seasons advanced the date of véraison and harvest but did not result in an increase in average daily temperatures during the ripening period. Harvest dates for Central Otago summer fruit were 2 weeks advanced in 2018 and a few days advanced in 2019 compared with normal.

In warm years, grain yields in wheat are reduced by the acceleration of crop development towards flowering and early harvest, as the crop has less time available to intercept sunlight and

convert it into biomass through photosynthesis. The change in flowering date also shifts the timing when the sensitive period to heat stress occurs, illustrating the interplay of both seasonal- and threshold-type damage effects in warm years (Rezaei et al. 2015). The final crop system response depends on various additional factors, including biotic stress and farmer's management choices such as genotype selection (Teixeira et al. 2018). Nevertheless, the general direction of yield changes suggests greater risk to spring wheat production in heatwave years. For potatoes, the two heatwave years caused significant losses in the production seasons in terms of yield and tuber quality.

Major species disruptions occurred in coastal marine ecosystems where bull kelp mortalities led to local extinctions and shifts in biodiversity.

Dedication Our good friend and colleague Dr Brett Mullan died during the final editing of this manuscript. He has made significant contributions and authored seminal papers in meteorology. These include the analysis of Southern Hemisphere climate and circulation variability over interannual (El Niño-Southern Oscillation) to interdecadal (Interdecadal Pacific Oscillation) timescales. The development of relationships with climate variability has been a basis for seasonal climate prediction for New Zealand commencing in the 1990s. Brett carried out pivotal research into climate change and modelling, emphasising on Southern Hemisphere and New Zealand regional effects. He has been a pioneer in producing climate change scenarios for New Zealand. He will be missed.

References

Arblaster JM, Meehl GA, Karoly DJ (2011) Future climate change in the southern hemisphere: competing effects of ozone and greenhouse gases. Geophys Res Lett 38(2). https://doi.org/10.1029/2010GL045384

Behrens E, Fernandez D, Sutton P (2019) Meridional oceanic heat transport influences marine heatwaves in the Tasman Sea on interannual to decadal timescales. Front Mar Sciee 6:228. https://doi.org/10.3389/fmars.2019.00228

Benthuysen J, Feng M, Zhong L (2014) Spatial patterns of warming off Western Australia during the 2011 Ningaloo Nino: quantifying impacts of remote and local forcing Cont. Shelf Res 91:232–246. https://doi.org/10.1016/j.csr.2014.09.014

Blunden J, Arndt DS (2019) A look at 2018 takeaway points from the state of the climate 2018 supplement. Bull Amer Met Soc 2019:1527–1538. https://doi.org/10.1175/BAMS-D-19-0193.1

Chinn TJ (2001) Distribution of the glacial water resources of New Zealand. J Hydrol N Z 40(2):139–187 https://www.jstor.org/stable/43922047

Chinn TJ, Fitzharris BB, Salinger MJ, Willsman A (2012) Annual ice volume changes 1976–2008 for the New Zealand Southern Alps. Glob Planet Change 92–93:105–118. https://doi.org/10.1016/j.gloplacha.2012.04.002

Compo GP, Whitaker JS, Sardeshmukh PD, Matsui N, Allan RJ, Yin X et al (2011) The twentieth century reanalysis project. Q J R Meteorol Soc 137(654):1–28. https://doi.org/10.1002/qj.776

de Lautour S (1999) The climatology of seasonal snow. MSc Thesis, Department of Geography, University of Otago

Dee DP, Uppala SM, Simmons AJ, Berrisford P, Poli P, Kobayashi S et al (2011) The ERA-interim reanalysis: configuration and performance of the data assimilation system. Q J R Meteorol Soc 137(656):553–597. https://doi.org/10.1002/qj.828

Fitzharris B, Garr GE (1995) Simulation of past variability in seasonal snow in the southern Alps, New Zealand. Ann Glaciol 21:377–382. https://doi.org/10.3189/S0260305500016098

Fogt RL, Perlwitz J, Monaghan AJ, Bromwich DH, Jones JM, Marshall GJ (2009) Historical SAM variability. Part II: twentieth-century variability and trends from reconstructions, observations, and the IPCC AR4 models. J Clim 22:5346–5365. https://doi.org/10.1175/2009JCLI2786.1

Garr CE, Fitzharris BB (1996) Using seasonal snow to forecast inflows into South island hydro lakes. In: Prospects and Needs for Climate Forecasting, The Royal Society of New Zealand Miscellaneous Series 34: 63–67 [ISBN 0-908654-61-8]

Gordon ND (1986) The southern oscillation and New Zealand weather. Mon Weather Rev 114:371–387. https://doi.org/10.1175/1520-0493(1986)114<0371:TSOANZ>2.0.CO;2

Greer DH, Weston C (2010) Heat stress affects flowering, berry growth, sugar accumulation and photosynthesis of *Vitis vinifera* cv. Semillon grapevines grown in a controlled environment. Funct Plant Biol 37:206–214. https://doi.org/10.1071/FP09209

Gregan P (2019) Vintage 2019 small but stunning. https://www.nzwine.com/media/13040/vintage-2019-small-but-stunning.pdf

Hartmann DL, AMG KT, Rusticucci M, Alexander LV, Brönnimann S, Charabi Y, Dentener FJ, Dlugokencky EG, Easterling DR, Kaplan A, Soden BJ, Thorne PW, Wild M, Zhai PM (2013) Observations: atmosphere and surface. In: Stocker TF, Qin D, Plattner K-G, Tignor M, Allen SK, Boschung J, Nauels A, Xia Y, Bex V, Midgley PM (eds) Climate Change 2013: The Physical Science Basis. Contribution of Working Group I to the Fifth Assessment Report of the Intergovernmental Panel on Climate Change. Cambridge University Press, Cambridge

Heidemann H, Ribbe J (2019) Marine heat waves and the influence of El Niño off Southeast Queensland, Australia, Frontiers of marine science, 20 February 2019. https://doi.org/10.3389/fmars.2019.0005d

Henley BJ, Gergis J, Karoly DJ, Power SB, Kennedy J, Folland CK (2015) A tripole index for the Interdecadal Pacific Oscillation. Clim Dyn 45(11–12):3077–3090. https://doi.org/10.1007/s00382-015-2525-1 Accessed on 05 27 2019 at https://www.esrl.noaa.gov/psd/data/timeseries/IPOTPI

Hiller L, Thornton RE (2008) Managing physiological disorders. Chapter 23: 235–246.In D. A. Johnson (Ed.), potato health management, 2nd edn. APS Press, Minnesota ISBN 978-0-89054-353-5

Hobday A, Alexander LV, Perkins SE, Smale DA, Straub SC, Oliver ECJ, Benthuysen JA, Burrows MT, Donat MG, Feng M, Holbrook NJ, Moore PJ, Scannell HA, Sen Gupta A, Wernberg T (2016) A hierarchical approach to defining marine heatwaves. Prog Oceanogr 141:227–238. https://doi.org/10.1016/j.pocean.2015.1012.1014 Outcome of Workshop #1

Hobday A, Oliver E, Gupta AS, Benthuysen J, Burrows M, Donat M, Holbrook N, Moore P, Thomsen M, Wernberg T, Smale D (2018) categorizing and naming marine heatwaves. Oceanogr 31(2)

Holzworth DP, Huth NI, deVoil PG, ZurcherEJ HNI, McLean G, Chenu K, van Oosterom EJ, Snow V, Murphy C, Moore AD, Brown H, Whish JM, Verrall S, Fainges J, Bell LW, Peake AS, Poulton PL, Hochman Z, Thorburn PJ, Gaydon DS, Dalgliesh NP, Rodriguez D, Cox H, Chapman S, Doherty A, Teixeira E, Sharp J, Cichota R, Vogeler I, Li FY, Wang E, Hammer GL, Robertson MJ, Dimes JP, Whitbread AM, Hunt J, van Rees H, McClelland T, Carberry PS, Hargreaves JNG, MacLeod N, McDonald C, Harsdorf J, Wedgwood S, Keating BA (2014) APSIM—evolution towards a new generation of agricultural systems simulation. Environ Model Softw 62. https://doi.org/10.1016/j.envsoft.2014.07.009

Huang B, Thorne PW, Banzon VF, Boyer T, Chepurin G, Lawrimore JH et al (2017) Extended reconstructed sea surface temperature, version 5 (ERSSTv5): upgrades, validations, and intercomparisons. J Clim 30(20): 8179–8205. https://doi.org/10.1175/jcli-d-16-0836.1

Jayne SR, Roemmich D, Zilberman N, Riser SC, Johnson KS, Johnson KC, Piotrowicz SR (2017) The Argo program: present and future. Oceanography 30:18–28. https://doi.org/10.5670/oceanog.2017.213

Kidson E (1935) The summer of 1934/35 in new Zealand NZ met.Office Note 16 12pp

Kidson JW (2000) An analysis of New Zealand synoptic types and their use in defining weather regimes. Int J Climatol 20(3):299–315. https://doi.org/10.1002/(SICI)1097-0088(20000315)20:3<299::AID-JOC474>3.0.CO;2-B

Kistler R, Collins W, Saha S, White G, Woollen J, Kalnay E et al (2001) The NCEP–NCAR 50–year reanalysis: monthly means CD–ROM and documentation. Bull Am Meteorol Soc 82(2):247–268. https://doi.org/10.1175/1520-0477(2001)082<0247:TNNYRM>2.3.CO;2

Levy D, Veilleux RE (2007) Adaptation of potato to high temperatures and salinity—a review. Amer J Potato Res 84:487–506. https://doi.org/10.1007/BF02987885

Marshall GJ (2003) Trends in the southern annular mode from observations and reanalyses. J Clim 16:4134–4143. https://doi.org/10.1175/1520-0442(2003)016<4134:TITSAM>2.0.CO;2

Molitor D, Junk J (2019) Climate change is implicating a two-fold impact on air temperature increase in the ripening period under the conditions of the Luxembourgish grapegrowing region. Oeno-one 3:409–422. https://doi.org/10.20870/oeno-one.2019.53.3.2329

Mullan AB, Stuart SJ, Hadfield MG, Smith MJ (2010) Report on the review of NIWA's 'Seven-Station' temperature series NIWA information series no. 78. 175 pp. https://www.niwa.co.nz/sites/niwa.co.nz/files/import/attachments/Report-on-the-Review-of-NIWAas-Seven-Station-Temperature-Series_v3.pdf

Mullan AB, Sood A, Stuart S (2016) Climate change projections for New Zealand: atmosphere projections based on simulations from the IPCC fifth assessment Wellington: Ministry for the Environment https://www.mfe.govt.nz/sites/default/files/media/Climate%20Change/Climate-change-projections-2nd-edition-final.pdf

Ojeda H, Deloire A, Carbonneau A (2001) Influence of water deficits on grape berry growth. Vitis 40:141–145 https://www.researchgate.net/publication/285702011_Influence_of_water_deficits_on_grape_berry_growth

Oliver ECJ, Benthuysen JA, Bindoff NL, Hobday AJ, Holbrook NJ, Mundy CN, Perkins-Kirkpatrick SE (2017) The unprecedented 2015/16 Tasman Sea marine heatwave. Nat Commun:8. https://doi.org/10.1038/ncomms16101

Oliver ECJ, Donat MG, Moore PJ, Smale DA, Alexander LV, Benthuysen JA, Feng M, Gupta AS, Hobday AJ, Holbrook NJ, Perkins-Kirkpatrick SE, Straub SC, Wernberg T (2018) Longer and more frequent marine heatwaves over the past century. Nat Commun 9:1324. https://doi.org/10.1038/s41467-018-03732-9

Parker AK (2012) Modelling phenology and maturation of the grapevine Vitis vinifera L.: Varietal differences and the role of leaf area to fruit weight ratio manipulations Lincoln University PhD thesis Lincoln University

Parker A, Garcia de Cortazar-Atauri I, Chuine I, Barbeau G, Bois B, Boursiquot J-M, Cahurel J-Y, Claverie M, Dufourcq T, Geny L, Guimberteau G, Hofmann RW, Jacquet O, Lacombe T, Monamy C, Ojeda H, Panigai L, Payan J-C, Lovelle BR, Rouchaud E, Schneider C, Spring J-L, Storchi P, Tomasi D, Trambouze W, Trought M, van Leeuwen C (2013) Classification of varieties for their timing of flowering and véraison using a modelling approach: a case study for the grapevine species Vitis vinifera L. Agric For Meteorol 180:249–264. https://doi.org/10.1016/j.agrformet.2013.06.005

Perkins-Kirkpatrick SE, King SE, Cougnon AD, Grosese EA, Oliver MR, Holbrook NJ, Lewis SC, Pourasghar F (2018) The role of natural variability and anthropogenic climate change in the 2017/18 Tasman Sea marine heatwave. Bull Am Meteorol Soc. https://doi.org/10.1175/BAMS-D-18-0116.1

Rezaei EE, Siebert S, Ewert F (2015) Intensity of heat stress in winter wheat—phenology compensates for the adverse effect of global warming. Environ Res Lett 10(24012). https://doi.org/10.1088/1748-9326/10/2/024012

Saha S et al (2006) The NCEP climate forecast system. J Clim 19:3483–3517. https://doi.org/10.1175/JCLI-D-12-00823.1

Salinger MJ (1979) New Zealand climate: the temperature record, historical data and some agricultural implications. Clim Chang 2:109–126. https://doi.org/10.1007/BF00133218

Salinger MJ, Diamond HJ (2020). Surface temperature trends in the New Zealand region 1871–2018. Submited to Weather and Climate

Salinger MJ, McGann RP, Coutts L, Collen B, Fouhy E (1992) South Pacific historical climate network. Temperature trends in New Zealand and outlying islands, 1920-1990. New Zealand meteorological service, 46pp, Wellington. ISBN 0-477-01598-0

Salinger MJ, Renwick JA, Behrens E, Mullan AB, Diamond HJ, Sirguey P, Smith RO, Trought MCT, Alexander LV, Cullen NC, Fitzharris BB, Hepburn CD, Parker AK, Sutton PJ (2019a) The unprecedented coupled ocean-atmosphere summer heatwave in the New Zealand region 2017/18: drivers, mechanisms and impacts. Environ Res Lett 14(4). https://doi.org/10.1088/1748-9326/ab012a

Salinger MJ, Chinn TJ, Fitzharris BB (2019b) Annual ice volume changes 1949–2019 for the New Zealand Southern Alps. Int J Climatol (submitted)

Siano AB, Roskruge N, Kerchkhoffs LHJ, Sofkova-Bobcheva S (2018) Yield and tuber quality variability in commercial potato cultivars under abiotic stress in New Zealand. Agron N Z 48:149–163 https://www.agronomysociety.nz/files/ASNZ_2018_14._Potato_yield_and_tuber_quality.pdf

Sutton PJ, Bowen M (2019) Ocean temperature change around New Zealand over the last 36 years. N Z J Mar Freshw Res 53(3):305–326. https://doi.org/10.1080/00288330.2018.1562945

Teixeira EI, de Ruiter J, Ausseil A-GA-G, Daigneault A, Johnstone P, Holmes A, Tait A, Ewert F (2018) Adapting crop rotations to climate change in regional impact modelling assessments. Sci Total Environ 616–617:785–795. https://doi.org/10.1016/j.scitotenv.2017.10.247

Thompson DWJ, Solomon S, Kushner PJ, England MH, Grise KM, Karoly DJ (2011) Signatures of the Antarctic ozone hole in southern hemisphere surface climate change. Nat Geosci 4(11):741–749. https://doi.org/10.1038/NGEO1296

Thomsen MS, South P (2019) Communities and attachment networks associated with primary, secondary and alternative foundation species; a case of stressed and disturbed stands of southern bull kelp. Diversity 11(4):56

Thomsen MS, Mondardini L, Alestra T, Gerrity S, Tait L, South PM, Lilley SA, Schiel DR (2019) Local extinction of bull kelp (Durvillaea spp.) due to a marine Heatwave. Front Mar Sci. https://doi.org/10.3389/fmars.2019.00084

Trenberth KE (1976) Fluctuations and trends in indices of the southern hemispheric circulation. Quart J Roy Met Soc 102(431):65–75. https://doi.org/10.1002/qj.4971024310

Trenberth KE, Zhang Y, Fasullo JT, Cheng L (2019) Observation-based estimates of global and Basin Ocean Meridional heat transport time series. J Clim 32:4567–4583. https://doi.org/10.1175/JCLI-D-18-0872.1

Trought MCT (2005) Fruitset - possible implications on wine quality. In: Kd G, Dundon C, Johnstone R, Partridge S (eds) Transforming flowers to fruit. Australian Society of Viticulture and Oenology, Mildura, pp 32–36

Troup AJ (1965) The 'southern oscillation'. Quart J Roy Met Soc 91(390):490–506. https://doi.org/10.1002/qj.49709139009

Affiliations

M. James Salinger[1] · Howard J. Diamond[2] · Erik Behrens[3] · Denise Fernandez[3] · B. Blair Fitzharris[4] · Nicholas Herold[5] · Paul Johnstone[6] · Huub Kerckhoffs[7] · A. Brett Mullan[3] · Amber K. Parker[8] · James Renwick[9] · Claire Scofield[6] · Allan Siano[7] · Robert O. Smith[10] · Paul M. South[11] · Phil J. Sutton[3,12] · Edmar Teixeira[6] · Mads S. Thomsen[13] · Michael C. T. Trought[14]

✉   M. James Salinger
     jimbosalinger09@gmail.com

[1]   Department Agriculture, Food, Environment and Forestry (DAGRI), University of Florence, 50144 Florence, Italy

[2]   NOAA/Air Resources Laboratory, College Park, MD 20740, USA

[3]   National Institute of Water and Atmospheric Research, Wellington, New Zealand

[4]   Department of Geography, University of Otago, Dunedin, New Zealand

[5]   The NSW Department of Planning, Industry and Environment, Science Division, Climate and Atmospheric Science, Parramatta, NSW, Australia

[6]   New Zealand Institute for Plant and Food Research Limited, Auckland, New Zealand

[7]   School of Agriculture and Environment, Massey University, Palmerston North, New Zealand

[8]   Department of Wine, Food and Molecular Biosciences, Lincoln University, Lincoln, New Zealand

[9]   School of Geography, Environment & Earth Sciences, Victoria University of Wellington, Wellington, New Zealand

[10]   Department of Marine Science, University of Otago, Dunedin, New Zealand

[11]   Cawthron Institute, Nelson, New Zealand

[12]   School of Environment, University of Auckland, Auckland, New Zealand

[13]   Centre of Integrative Ecology and the Marine Ecology Research Group, School of Biological Sciences, University of Canterbury, Christchurch, New Zealand

[14]   Innovative Winegrowing, Blenheim, New Zealand